Formation and Development of Nocturnal Boundary Layer Clouds over the Southern Great Plains

PING ZHU, BRUCE ALBRECHT, AND JON GOTTSCHALCK

MPO/RSMAS, University of Miami, Miami, Florida

(Manuscript received 20 August 1999, in final form 27 April 2000)

ABSTRACT

The formation and evolution of nocturnal boundary layer clouds over land are studied using a simple well-mixed boundary layer theory. By analyzing the deepening rate of the mixed layer depth based on the turbulent kinetic energy budget of the whole boundary layer, the authors studied how the formation of idealized nocturnal boundary layer clouds is related to the physical processes associated with the land surface and the boundary layer. Preliminary analysis indicates that for a range of surface moisture and heat fluxes, wind shear can be an important factor in triggering the formation of nocturnal stratus. The relative importance of different physical processes responsible for cloud formation can be evaluated by the ratio between the lifting condensation level and a critical level, which is proportional to the Monin-Obukhov length scale. In this study, data collected from the Atmospheric Radiation Measurement site in the southern Great Plains are used to examine the results of the theoretical analysis. The analyses of the two nocturnal stratus cloud cases observed on 25 October 1996 and 6 November 1997 indicate that the turbulent mixing induced by the wind shear plays a pivotal role in the cloud formation during these two cases.

1. Introduction

Boundary layer clouds can form at the top of the mixed layer, and are frequently observed on the east side of the oceans, over polar regions, and over land in midlatitudes. Those over oceans, usually taking the form of stratus and stratocumulus, cover extensive areas, and can persist for a long time. Because of their high albedo and a cloud-top temperature similar to that of the underlying surface, these clouds have been widely recognized as an important factor in modulating the earth's radiation budget, and thus can have a strong effect on regional and global climate. In contrast, the boundary layer clouds over land in the midlatitudes are important for their strong influence on local weather, their effects on the diurnal cycle, and their interaction with trace gases that can complicate air pollution problems such as chemical reaction rates and the removal of pollutants from the boundary layer. Furthermore, representing the diurnal cycle of continental low-level clouds in large-scale and regional models can be important to the accuracy of the numerical simulations. Therefore, understanding the processes governing the low-level clouds is critical to both climate problems and local weather. However, since the cloud-topped boundary layer is a rather complex phenomenon that depends on the interaction of many processes, such as longwave radiative cooling occurring at cloud top, the entrainment processes, surface processes, synoptic-scale subsidence, wind shear, and the microphysics of the clouds themselves, many questions still need to be answered before we can get a clear picture of how these clouds influence weather and climate.

Among all the issues related to boundary layer clouds, cloud formation is perhaps the most fundamental question, but has received little attention. From Lilly's (1968) classic mixed layer model to multilayered models (Betts 1973; Albrecht 1979; Wang 1993), clouds or even cloud structure is artificially prescribed in the model at the initial time. The limitations of these models, however, restrict their use to study cloud formation problems. Even with large eddy simulations (LES), researchers (Moeng 1986; Moeng et al. 1992, 1999; Stevens et al. 1998) mostly focus on questions related to the maintenance of cloud-topped boundary layers rather than cloud formation. Observational analyses (e.g., Rogers et al. 1995b; Duynkerke et al. 1995) have a similar bias. This bias is probably due to historical reasons, since most of the field experiments, such as the Atlantic Stratocumulus Transition Experiment (Albrecht et al. 1995) and the First ISCCP (International Satellite Cloud Climatology Project) Regional Experiment (Albrecht et al. 1988), focused on marine stratus and stratocumulus clouds, as well as trade wind cumuli that are persistent almost all year round. The importance of

Corresponding author address: Ping Zhu, MPO/RSMAS, University of Miami, 4600 Rickenbacker Causeway, Miami, FL 33149-1098. E-mail: pzhu@rsmas.miami.edu.

cloud formation is generally overshadowed by other issues such as cloud maintenance, interaction of the clouds with the boundary layer and the free atmosphere, and their influence on the large-scale dynamics.

Compared with the substantial efforts on marine boundary layer cloud systems, however, continental boundary layer clouds are relatively overlooked despite the fact that they are more observationally accessible to us than marine clouds (Del Genio et al. 1996). The formation of continental boundary layer clouds are complicated not only by changes of the thermodynamic and hydrological conditions of the land surface due to the precipitation and other weather events, but also by geographical factors, such as terrain and variations in the sources and abundance of cloud condensation nuclei. The diversity of these clouds implies that the major mechanisms responsible for cloud formation may vary under different conditions. Thus, for continental boundary layer clouds, cloud formation could be as important as other cloud-related issues.

In this paper, we are concerned primarily with the evolution of nocturnal boundary layer (NBL) clouds. One question that has not been adequately addressed is what are the major mechanisms that form boundary layer clouds during the evening? In other words, how do these clouds form under statically stable stratification? One possibility is that these clouds form during the daytime, and then persist through the night (Rogers et al. 1995b). However, we do find many cases during the Atmospheric Radiation Measurement (ARM) field observations over the southern Great Plains (SGP) that stratus clouds form in the middle of night (Fig. 5 shows an example of one of these cases). Obviously, another possibility is that these clouds can be advected from elsewhere by processes such as frontal passages, or mesoscale systems. Observations show, however, that the cloud bases and the lifting condensation levels (LCL) calculated from surface meteorological data are often coupled. Thus, it is reasonable to ask if there is any possibility that these clouds are produced by the boundary layer processes themselves? Answering this question can help illuminate the basic physics related to the clouds, the boundary layer, and the interaction between them.

In the daytime, the clouds at the top of the mixed layer over land are often little more than tracers of the preexisting thermals produced by positive buoyancy that can be traced to the lowest part of boundary layer, a situation that Stull (1985) called forced clouds. The relationship between low-level clouds, the height of the mixed layer, and the LCL proposed by Deardorff et al. (1980) provides the framework for considering issues associated with the cloud-topped boundary layer. Unlike the convective boundary layer (CBL), in the evening there is no solar radiative heating at the underlying surface to produce positive buoyancy. Furthermore, longwave radiative cooling at the surface results in negative buoyancy that suppresses turbulent mixing. In this case, it would be difficult to form NBL clouds by the same mechanisms that operate in the daytime. The radiatively driven, stable boundary layer over land has been the focus of a large number of theoretical and observational studies such as Caughey et al. (1979), Nieuwstadt (1984), Sorbjan (1986, 1987), and Garratt (1987). Although these studies contribute substantially to our understanding of the mechanisms for the clear NBL, they do not consider the cloud-topped NBL.

Turbulence within the boundary layer can also be generated and maintained by wind shear, particularly under neutral and stable boundary layer conditions. As Zeman (1979) noted, shear is sometimes the sole source of turbulence, and in the absence of shear a turbulent boundary layer cannot survive. In this case, the growth or decay of the NBL depends on an interaction between the shear-driven turbulence and the consumption of turbulence due to negative buoyancy forces (Rogers et al. 1995a). As a result, if we consider the mechanisms for forming NBL clouds, the surface wind shear must be taken into account, especially in the initial stage of cloud formation. At one extreme, strong winds, strong turbulence, and weak surface cooling can lead to a well-mixed layer in the NBL that behaves in a bulk sense similar to a CBL as described by Stull (1988). In this case, the moisture in the lower levels can also be efficiently transported upward due to mixing produced by turbulence. Specifically, if the boundary layer deepens to a level above the LCL due to turbulent mixing, then it is possible to form clouds at the boundary layer top. One objective of this paper is to determine the conditions that can support forced (shear-driven) NBL clouds over land. Since the LCL is much lower at night than in the daytime, and there are no convective thermals in the evening due to negative buoyancy, the NBL clouds are usually low and take the form of stratus as we often observe in many places. The nocturnal cloud formation problem is of further interest since a similar mechanism may be responsible for the formation of marine stratus or stratocumulus in the regions where surface buoyancy fluxes are small and wind shear is strong.

In this study, the conditions necessary to form forced NBL clouds, and the factors controlling the deepening rate of the NBL are analyzed in sections 2 and 3. In section 4, we will examine the basic relations and conditions derived in sections 2 and 3 using the data collected at the ARM SGP site. In the last section we will discuss a few related questions based on the data analysis.

2. Conditions for the formation of NBL clouds

According to Stull (1985), the simple, but fundamental condition for forming forced boundary layer clouds under well-mixed conditions is that the LCL is lower than the boundary layer height (h) since these clouds are merely visible tracers of mixing within the boundary layer. Based on observations and a theoretical

analysis, Lilly (1968) argued that since the Monin-Obukhov length scale is usually small, not often greater than a few tens of meters, the surface wind shear may not be important for the maintenance of a mixed layer of 500–1000 m or more in thickness. Therefore, wind shear is usually considered to be a minor factor in the development of the CBL. However, under nocturnal conditions, wind shear is the only source of turbulent production before cloud formation. Thus, it is important to know how dynamic and thermodynamic processes control the development of the NBL, especially under strong wind conditions, which can also result in mixed layers, but with a different turbulent anisotropy from that in the CBL. The turbulent structures in free convection are predominately vertical, while, in forced shear convection, the eddies are sheared into a much more horizontal or slanting orientation, and probably with a more chaotic appearance. But as Zeman (1979) stated, on many occasions information on details of the turbulence are not necessary, since only the bulk effects of the turbulence on the boundary layer are important. As long as the well-mixed conditions are met, the relationship between low-level clouds, the boundary layer height, and the LCL is still applicable to the NBL as confirmed by many observations.

In this study, we focus on conditions for the formation of NBL clouds. It is the integral properties of the boundary layer such as the depth of boundary layer, bulk wind and temperature, and surface fluxes that must be considered. A logical way to begin this analysis is to study the turbulent kinetic energy (TKE) budget of the entire boundary layer. For the homogeneous situation, under the assumption that the turbulent field approaches steady state, choosing a coordinate system aligned with the mean wind, and neglecting subsidence, then the TKE budget equation can be written as

$$0 = \frac{g}{\overline{\theta_v}}\overline{w'\theta_v'} - \overline{w'u'}\frac{\partial \overline{U}}{\partial z} - \frac{\partial}{\partial z}\overline{\left[w'\left(\frac{p'}{\overline{\rho}} + e\right)\right]} - \varepsilon, \quad (1)$$

where ρ is the density of air, e is the mean turbulent kinetic energy, θ_v is the virtual potential temperature, u and w are horizontal and vertical wind velocity, p is the atmospheric pressure, and g is the acceleration due to gravity. The overbar and prime here indicate the mean and perturbation parts of any physical fields, respectively. The first, second, third, and fourth term on the right-hand side of Eq. (1) represent the buoyant production or consumption term, the mechanical or shear production term, the pressure correlation and turbulent transport term, and the viscous dissipation term, respectively. A simplified form of Eq. (1) can be obtained by integrating this equation over the depth of the boundary layer and applying simple mixed layer theory.

a. Buoyant production and consumption

It is easy to show that the turbulent heat fluxes must have a linear variation with height if θ_v is constrained to be well mixed with height. Thus, we can write

$$\overline{w'\theta_v'} = \overline{w'\theta_{v0}'} + \frac{z}{h}\left(\overline{w'\theta_{vh}'} - \overline{w'\theta_{v0}'}\right), \quad (2)$$

where h is defined as the mixed layer depth, and the right-hand subscripts "0" and "h" represent the flux at the surface and at the top of the mixed layer. Integrating Eq. (2) through the depth of the mixed layer, gives

$$\int_0^h \frac{g}{\overline{\theta_v}}\overline{w'\theta_v'}\,dz = \int_0^h \frac{g}{\overline{\theta_v}}\left[\overline{w'\theta_{v0}'} + \frac{z}{h}\left(\overline{w'\theta_{vh}'} - \overline{w'\theta_{v0}'}\right)\right]dz$$

$$= \frac{gh}{2\overline{\theta_v}}\overline{w'\theta_{v0}'} - \frac{gh}{2\overline{\theta_v}}W_e\Delta\overline{\theta_v}. \quad (3)$$

To get Eq. (3), we have used the relation

$$-\overline{w'\theta_{vh}'} = W_e\Delta\overline{\theta_v}, \quad (4)$$

where W_e is defined as the entrainment velocity, and $\Delta\overline{\theta_v}$ is the difference of the virtual potential temperature across the inversion zone capping the mixed layer, that is, $\Delta\overline{\theta_v} = \overline{\theta_v}^{+h} - \overline{\theta_v}^{-h}$. For conditions where the large-scale subsidence is negligible, we note that

$$W_e = \wedge\frac{\partial h}{\partial t},$$

where $\wedge$ is the Heaviside unit function defined as

$$\wedge = \begin{cases} 1 & \text{if } \dfrac{\partial h}{\partial t} > 0 \\ 0 & \text{if } \dfrac{\partial h}{\partial t} < 0, \end{cases}$$

which means entrainment is always associated with mixed layer deepening, otherwise the second law of thermodynamics will be violated.

b. Shear production

The shear production term is not as easy to treat as the buoyant production term. For the forced convection case, wind shear is important. It is thus imperative that in NBL models the shear be represented realistically. In the NBL the greatest wind shear magnitude usually occurs at the surface. Not surprisingly, the maximum shear production rate for turbulence also occurs there. Thus, shear near the surface is usually more important for generating mixing than shear above the surface layer (Stull 1988). Without strong surface wind shear, maintenance of a mixed layer above the surface layer is impossible. Based on the structure of the shear-driven NBL, we shall divide the entire NBL into three parts—the surface layer, the outer layer (above the surface layer but below the top of the NBL), and the transition zone at the NBL top. Thus the integration of the shear production term in Eq. (1) gives

$$\int_0^h -\overline{w'u'}\frac{\partial \overline{U}}{\partial z}\,dz = \int_0^{d_s} -\overline{w'u'}\frac{\partial \overline{U}}{\partial z}\,dz + \int_{d_s}^{h-} -\overline{w'u'}\frac{\partial \overline{U}}{\partial z}\,dz + \int_{h-}^{h+} -\overline{w'u'}\frac{\partial \overline{U}}{\partial z}\,dz, \quad (5)$$

where d_s is the depth of the surface layer.

Within the surface layer (d_s), similarity theory yields

$$\overline{w'u'} \propto U_*^2; \qquad \frac{\partial \overline{U}}{\partial z} \propto U_*, \quad (6)$$

where U_* is the frictional velocity.

In the outer layer, the wind is treated uniformly like a slab as we do for the virtual potential temperature so that

$$\frac{\partial \overline{U}}{\partial z} = 0. \quad (7)$$

Note that Eq. (7) is highly idealized in a slab model. In the real boundary layer, $\partial\overline{U}/\partial z$ is small but may not be zero. Since the overall shear production of this part is much smaller than the first term in Eq. (5), Eq. (7) is a very good approximation for the mixed layer (outer layer) in a shear-driven NBL.

In the transition zone at the top of the boundary layer, similar to Eq. (4), the momentum flux boundary condition can be expressed as (Kraus 1977)

$$\overline{w'u'}_h + W_e\Delta\overline{U} = 0, \quad (8)$$

where $\Delta\overline{U}$ is the velocity difference across the inversion zone, that is, $\Delta\overline{U} = U^{+h} - U^{-h}$. Then Eq. (5) with Eqs. (6), (7), and (8) becomes

$$\int_0^h -\overline{w'u'}\frac{\partial \overline{U}}{\partial z}\,dz = \alpha_1 U_*^3 + 0 + \int_{h-}^{h+} W_e\Delta\overline{U}\frac{\partial \overline{U}}{\partial z}\,dz = \alpha_1 U_*^3 + \int_{u-}^{u+} W_e\Delta\overline{U}\,dU = \alpha_1 U_*^3 + W_e\Delta\overline{U}^2, \quad (9)$$

where α_1 is an empirically determined proportionality parameter.

c. Turbulent transport and pressure correlation

The quantity $\overline{w'e}$ in Eq. (1) represents the vertical turbulent flux of TKE. On a local scale, $-\partial/\partial z(\overline{w'e})$ may act as either production or damping of turbulence, depending on whether there is turbulent flux convergence or divergence. When integrated over the whole boundary layer, $\int_0^h -(\overline{w'e})\,dz$ will become zero provided that the boundaries are not turbulent. In this case, this term neither creates nor destroys TKE, it just redistributes TKE within the boundary layer.

In the stable boundary layer regime, perturbations are associated with turbulence as well as waves. Stull (1988) suggested that turbulent energy can be lost from the boundary layer top in the form of internal gravity waves excited by the turbulence penetrating the stable layer at the top of the boundary layer. Thus, the pressure correlations not only act to redistribute TKE within the boundary layer like the turbulent transports, but they may also transport energy out of the boundary layer. However, the value of this term is extremely difficult to estimate since the magnitudes of these fluctuations are very small. For simplicity, following Kraus (1977), we shall describe the pressure correlation term and turbulent transport term as

$$-\int_0^h \frac{\partial}{\partial z}\overline{\left[w'\left(\frac{p'}{\overline{\rho}} + e\right)\right]}\,dz = W_e\Delta e - \alpha_2 U_*^3, \quad (10)$$

where Δe is the kinetic turbulent energy across the inversion zone, that is, $\Delta e = e^{+h} - e^{-h}$, and α_2 is an another empirically determined proportionality parameter. Although our understanding of the vertical distribution of TKE in the boundary layer is limited due to measurement difficulty, we might expect that Δe is very small, since simulations based on Wangara data (Therry and Lacarrere 1983) show TKE often decreases with height from a maximum value, which is at a height of about $z/h \approx 0.3$ for a CBL, and at a height just above the surface for nocturnal conditions.

d. Dissipation

For most second-order turbulent closure models, the viscous dissipation has to be parameterized. From dimensional arguments, dissipation can be expected to be proportional to the third power of the frictional velocity. The turbulent agitation is most intense close to the regions where turbulent energy is generated. For example, when the turbulence is generated due to wind stirring, its intensity tends to decrease with the distance from the surface. On the basis of this argument, it will be assumed here that the dissipation integral is proportional to the active turbulence generating processes, and can be parameterized as

$$\int_0^h \varepsilon\,dz = \alpha_3 U_*^3, \quad (11)$$

where α_3 is another empirically determined proportionality constant.

If we neglect Δe, and then combine Eqs. (3), (9), (10), and (11), we get

$$\wedge\frac{\partial h}{\partial t} = \frac{1}{\frac{gh}{2\overline{\theta}_v}\Delta\overline{\theta}_v - \Delta\overline{U}^2}\left(\frac{gh}{2\overline{\theta}_v}\overline{w'\theta'_v}_0 + \alpha U_*^3\right), \quad (12)$$

where α is defined as $\alpha = \alpha_1 - \alpha_2 - \alpha_3$. We will discuss how to determine α in section 3.

Equation (12) is similar to that in the classic Kraus and Turner (1967) model, which is often used to treat the oceanic mixed layer. This is not surprising since the basic physics for the wind-driven nocturnal atmospheric boundary layer is the same as the wind-driven oceanic mixed layer. The only major difference here is that the atmospheric boundary layer wind increases with height, while the velocity goes approximately to zero when approaching the bottom of the oceanic mixed layer. Thus, for the oceanic mixed layer, we can simply neglect the velocity term. For the atmospheric boundary layer, although observations show that the velocity difference across the boundary layer top is usually small, exceptions may exist. We shall keep this term in Eq. (12) for further analysis.

If we rewrite Eq. (12) in the following form:

$$\alpha U_*^3 = -\frac{gh}{2\overline{\theta}_v}\overline{w'\theta'_{v0}} + \wedge\frac{\partial h}{\partial t}\left(\frac{gh}{2\overline{\theta}_v}\Delta\overline{\theta}_v - \Delta\overline{U}^2\right), \quad (13)$$

(1) (2) (3) (4)

then the physics behind this equation is pretty clear. Equation (13) indicates that for the forced, well-mixed boundary layer, the net rate of mechanical production of turbulence, which is term (1) in Eq. (13), should balance the net rate of buoyant damping of turbulence induced by the surface heat flux, which is term (2) in Eq. (13), and the damping or production of turbulence produced by the entrainment mixing near the top of the mixed layer, which is represented by term (3) and term (4) in Eq. (13). The value of term (3) depends on the strength of the inversion layer, which suppresses the turbulence unless there is buoyancy reversal in a cloudy boundary layer. The magnitude of term (4), which is always related to turbulence production, is determined by the strength of the wind shear across the inversion layer.

The simple formulation given by Eq. (12) or Eq. (13) illustrates the basic physics for a shear-driven NBL. From Eq. (12), we see that in order for the Heaviside condition to be met, in other words, deepening the depth of NBL, both numerator and denominator in Eq. (12) have to be either positive or negative. The first case is

$$\begin{cases} \dfrac{gh}{2\overline{\theta}_v}\overline{w'\theta'_{v0}} + \alpha U_*^3 > 0 & (14a) \\ \dfrac{gh}{2\overline{\theta}_v}\Delta\overline{\theta}_v - \Delta\overline{U}^2 > 0. & (14b) \end{cases}$$

From Eq. (14a), we get

$$h = -\frac{2\overline{\theta}_v\alpha U_*^3}{g\overline{w'\theta'_{v0}}} = 2\alpha k L_{ob} > 0, \quad (15)$$

where $L_{ob} = -\overline{\theta}_v U_*^3/gk\overline{w'\theta'_{v0}}$ is Monin-Obukhov length scale, k is the von kármán constant. We note that the Monin-Obukhov length scale is greater than zero, which means the NBL is statically stable. Physically this makes sense. In this study, we will focus on this case. Equation (14b) indicates that the velocity difference across the top of the boundary layer should be small. For the cases that we analyze in section 4, sounding profiles do show that the velocity across the top of the boundary layer is small (not shown here). We believe this is the normal situation for the NBL.

Equation (14) indicates that the depth of NBL must deepen with time to satisfy this condition. As time goes on, the downward surface buoyancy heat flux is getting stronger and stronger due to surface radiative cooling, and eventually the buoyant damping due to surface cooling alone will balance the wind-stirring term. When this happens, the depth of the NBL will stop growing, and we have

$$\frac{gh}{2\overline{\theta v}}\overline{w'\theta'_{v0}} + \alpha U_*^3 = 0, \quad (16)$$

which gives us a critical level:

$$h_{crit} = -\frac{2\overline{\theta}_v\alpha U_*^3}{g\overline{w'\theta'_{v0}}} = 2\alpha k L_{ob}. \quad (17)$$

This critical level can be seen as the upper limit of the depth of the NBL that can develop for given surface fluxes and wind stresses, or we can say that this is the maximum height that surface layer air can reach due to turbulent mixing. Furthermore, if this critical level is greater than the LCL of the surface layer air, then, clouds could form and develop. This is the sufficient condition for the formation of NBL clouds. The above analysis results in a very important dimensionless parameter, namely, the ratio between the LCL and the critical level, which can be used to diagnose the possibility of the formation of NBL clouds:

$$R_0 = \frac{h_{crit}}{Z_{lcl}} = -\frac{2\overline{\theta}_v\alpha U_*^3}{g\overline{w'\theta'_{v0}}Z_{lcl}} = \begin{cases} \text{possible cloudy} & \text{if } R_0 > 1 \\ \text{clear} & \text{if } R_0 < 1. \end{cases} \quad (18)$$

Basically, this ratio combines the different influences of dynamic, thermodynamic, and moisture processes (U_*, $\overline{w'\theta'_{v0}}$, LCL) that control the formation of NBL clouds, and can also be used to evaluate the relative importance of these processes on cloud formation. In addition, if the LCL is very low, which means the surface layer is almost saturated, then it may be possible to form fog in the stable boundary layer.

Mathematically, there is another condition for which the Heaviside in Eq. (12) equals 1, and there is a possibility for subsequent growth of the mixed layer. This condition is

$$\begin{cases} \dfrac{gh}{2\overline{\theta}_v}\overline{w'\theta'_{v0}} + \alpha U_*^3 < 0 & \text{(19a)} \\ \dfrac{gh}{2\overline{\theta}_v}\Delta\overline{\theta}_v - \Delta\overline{U}^2 < 0. & \text{(19b)} \end{cases}$$

From Eq. (19a), we get

$$h = \frac{-2\overline{\theta}_v \alpha U_*^3}{g\overline{w'\theta'_{v0}}} = 2\alpha k L_{ob} < 0, \qquad (20)$$

which indicates that the Monin-Obukhov length scale is negative in this condition. Since the Monin-Obukhov length scale has to be positive in the stable NBL; thus under the condition of Eq. (19), Eq. (12) physically may describe one of the situations for the development of the daytime CBL, in which the Monin-Obukhov length scale is negative. From Eq. (19b), we see that under this condition, the wind shear across the transition zone at the boundary layer top should be large, which may lead to so-called top–down convection, a conception usually used to describe the daytime CBL in order to decompose the passive and active fields (Sorbjan 1999). However, this case is beyond the scope of the statically stable NBL that is the focus of this study.

From the above analysis, we see that the condition for the development of the NBL is very strict. Equation (14) is the condition under which the development of the NBL is possible. We may diagnose the formation of NBL clouds since only under this condition are the bulk characteristics of the NBL closely related to the wind shear and the surface fluxes. Under many other conditions our analysis may fail since weak surface wind shear results in a decoupling of surface processes from the upper part of the boundary layer. In other words, the bulk characteristics of the NBL have no simple relationship with the wind shear and surface fluxes. This well-known difficulty of treating the stable boundary layers motivates many studies. The wide variety of NBL flow states has resulted in a number of idealized models for describing the NBLs. No single model works for all situations. The purpose of this study is to illustrate the basic physics for the formation of NBL clouds using a simple slab model. The model seems to work well here.

The validity of Eq. (12) can also be seen from its capability to represent the normal situation of the daytime CBL in which the surface sensible heat flux is strong and positive, but the mechanical turbulent production is small, and usually can be neglected. If the velocity difference across the top of the boundary layer is small, which is often true in the daytime CBL, then Eq. (12) reduces to Eq. (4) under Ball's hypothesis (Lilly 1968). This is the equation that describes the development of the CBL, and is well-described in the literature (Garratt 1992).

The relationship between the LCL and the critical level may also be used to explain how clouds form over the ocean surface in areas of high wind but weak surface fluxes. For example, off the coast of California, the air temperature often closely tracks the SST, with air temperature between 0.5°C and 1.0°C cooler than the SST (Stephen and Hartmann 1993). With this small air–sea temperature difference, weak surface fluxes alone may not be responsible for the formation of stratus clouds, rather, it is possible that wind shear triggers the formation of these stratus clouds.

3. Determination of α

The preceding analysis involves a very important proportionality factor α, which has to be established empirically. Unfortunately, no experimental work has been done previously to determine the factor α in the atmospheric boundary layer. Although oceanographers for convenience treat this factor as a constant in many oceanic models, this may not be true in the atmosphere since the TKE budget analyses presented by Deardorff (1974), Andre et al. (1978), Terry and Lacarrere (1983), Lenschow (1974), Zhou et al. (1985), and Chou et al. (1986) show that the net combined effect of the shear production, transport, pressure correlation, and dissipation of turbulence is related to the stability. Thus, α should be a function of the stability of the boundary layer, that is, $\alpha = \alpha(\mathrm{Ri})$ or $\alpha = \alpha(L_{ob})$. Here Ri and L_{ob} represent the Richardson number and the Monin-Obukhov length scale.

In this study, we design a numerical experiment to determine the factor α for the nocturnal boundary layer based on the TKE budget equation, which can be written as

$$\frac{de}{dt} = -\overline{u_i' u_j'}\frac{\partial \overline{U}_i}{\partial x_j} + \frac{g}{\overline{\theta}}\overline{w'\theta'_v} - \frac{\partial}{\partial x_i}\overline{\left[u_i'\left(e + \frac{p'}{\rho_0}\right)\right]} - \varepsilon. \qquad (21)$$

Equation (1) is the simplified form of Eq. (21). Based on the derivation in section 2, the factor α can be expressed as

$$\alpha = \frac{1}{U_*^3}\left(\int_0^h \left[-\overline{u_i' u_j'}\frac{\partial \overline{U}_i}{\partial x_j}\right] dz - \int_0^h \frac{\partial}{\partial x_i}\overline{\left[u_i'\left(e + \frac{p'}{\rho_0}\right)\right]} dz - \int_0^h \varepsilon\, dz\right), \qquad (22)$$

where U_*^3 and the integrals can be calculated using a layered atmospheric model, and h is defined in this experiment as the level where TKE drops to 20% of its value near the surface.

The basic numerical model used in this study is a two-dimensional homogeneous version of the Regional Atmospheric Modeling System (RAMS). A detailed description of the RAMS model is given by Pielke et al.

(1992). The basic model setup features are: nonhydrostatic, compressible equations in a σ_z coordinate system with a hybrid numerical scheme and cyclic lateral and Klemp-Durran top boundary conditions. The Surface-layer parameterization used in the model is the Louis *scheme (1979), which determines the fluxes from the surface into the atmosphere. This scheme approximates the profile functions of Businger et al. (1971). The level-2 1/2 high-order turbulent closure scheme described by Mellor and Yamada (1982) is adopted here as the turbulent closure scheme. A variable vertical grid mesh spacing with the lowest level at 15 m and an expansion ratio of 1.07, and a horizontal grid mesh spacing with 5000 m are used in this simulation. The initial condition for this simulation is the neutral state with an upper boundary velocity of 15 m* s^{-1} (a velocity equivalent to the geostrophic wind at the top boundary). The surface thermodynamic boundary condition is a simple one that specifies a constant temperature difference between a fictitious soil temperature and the temperature of the lowest level of the atmosphere. This specification provides a simple way to impose a surface source or sink of energy to the atmosphere. For example, a ground surface temperature lower than the air temperature above is equivalent to imposing a flux of heat into the surface. One advantage of this boundary condition, according to Wyngaard (1975), is that the mean state of the simulated boundary layer can approach a quasi-steady state. In this study, different prescribed temperature differences are chosen to obtain a wide range of stability conditions. The simulation time for each run is 100 h. The Monin-Obukhov length scale and α were calculated every half-hour using the output of the RAMS model, and the values for the last 60 h of the simulations are plotted in Fig. 1 (each family of dots corresponding to the simulation with different prescribed temperature differences, such as 0.1°C, 0.2°C. . .). Simulations show that after 40 h, the mean fields are almost time independent. The results in Fig. 1 indicate that the variability of the values (family of dots) for the last 60 h increases with a decrease of the Monin-Obukhov length scale, especially when the stability of the NBL gets stronger (smaller Monin-Obukhov length scale). Since α and the Monin-Obukhov length scale were calculated from high-order turbulence variables, the turbulent field is not steady with small Monin-Obukhov length scale, which is different from the mean state (quasi-steady-state). This phenomenon is so-called intermittent turbulence or discontinuous turbulent processes in the stable boundary layer (Stull 1988). One reason for the intermittent turbulence is that the NBL is too stable to produce enough turbulent mixing.

The same numerical experiment is done using Deardorff's (1980) TKE turbulent closure scheme but with a smaller horizontal grid mesh ($\Delta x = 100$ m). Similar results are obtained. The grid size of this numerical experiment indicates that our simulations are basically

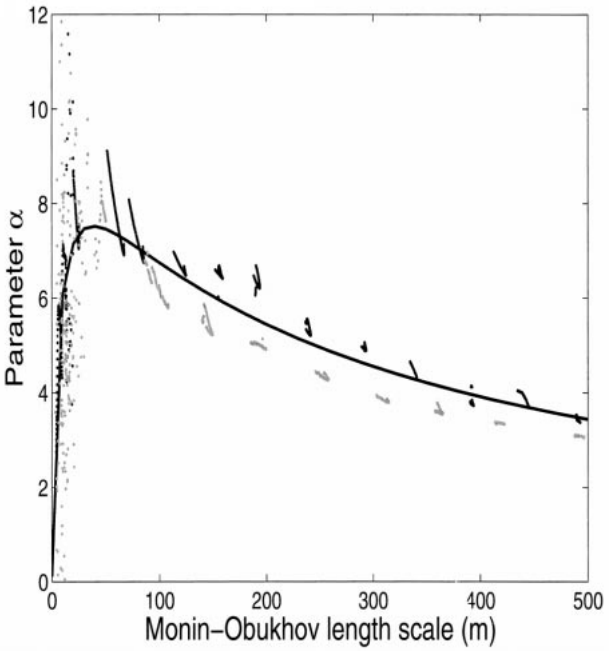

FIG. 1. Simulated proportionality factor α vs the Monin-Obukhov length scale L_{ob} and the fitting curve. Light dots: Deardorff's scheme with small horizontal grid size (100 m). Dark dots: Mellor and Yamada's scheme with large horizontal grid size (5000 m). Each family of dots is obtained from the simulated results (obtained every 30 min to give total 120 points) for the last 60 h.

LESs that resolve the large eddies but parameterize the small eddies. Since small eddies contribute much less heat and momentum transport than large eddies, and are less flow-dependent and more isotropic (Moeng, 1984), the simulation results should not be sensitive to the parameterization schemes that parameterize only the small eddies.

With the relation between the factor α and the Monin-Obukhov length scale L_{ob}, it is easy to calculate the critical level using surface meteorological data and flux data with Eq. (17). The critical level from this calculation can then be compared with the LCL calculated from surface temperature and moisture data.

4. Case study results

a. Description of the ARM site and instrumentation

The data that we used were collected at the ARM SGP site. This site covers a 365 km (north–south) × 300 km (east–west) area (about 110 000 km^2) that extends from south-central Kansas to central Oklahoma. The topography of the research area is rather flat, therefore we may neglect mesoscale circulations induced by local terrain. The SGP site includes a central facility, four boundary facilities, three intermediate facilities, and more than twenty extended facilities. Figure 2 shows the locations of the observational facilities used in this study and the local topography. The central fa-

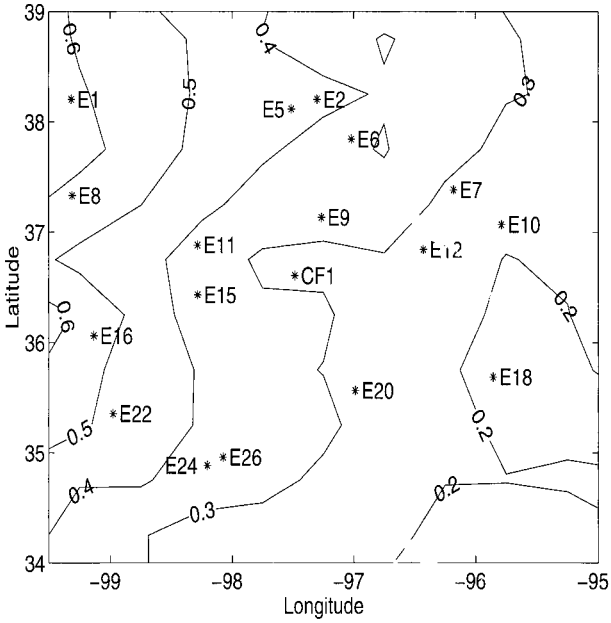

FIG. 2. The locations of observational facilities indicated by stars at the ARM SGP site. The Eddy Correlation Flux Measurement System (ECOR) is deployed at CF1, E1, E6, E10, E16, and E24, and the Energy Balance Bowen Ratio System (EBBR) at the rest of the facilities. The contours (km) indicate the topography of the research area.

cility, which is where most of the instrumentation is deployed, is located near Lamont in north-central Oklahoma (36°36′N, 97°29′W, and 320 m above sea level), 50 km south of the Kansas border. Extensive suites of instruments are deployed at these facilities to observe and detect a wide range of atmospheric parameters.

The instrumentation includes a wide array of conventional and state-of-the-art observing systems that include the following functions: measure vertical profiles of wind, temperature, and water vapor; quantify cloud cover, cloud liquid water content, and ice mixing ratio; and observe surface fluxes of heat and moisture. The instruments and the related observed atmospheric parameters are described in Table 1.

b. Synoptic conditions

In this study, two NBL cloud cases were studied based on the analysis and derivation made in section 2. These two cases were observed on 25 October 1996 and 6 November 1997. For 25 October 1996, the Geostationary Operational Environment Satellite (GOES) IR image shows a large clear area around the observational site at 0000 UTC (1900 LST, Fig. 3a). The surface weather map at this time (Fig. 3b) shows a low pressure center over eastern Colorado while the southeastern part of the United States is under high pressure. The observational site is on the boundary of these two systems. The surface weather map and satellite image at 1200 UTC (0700 LST) 25 October (not shown here) indicate that the low pressure system was nearly stationary, and did not substantially affect the research area.

For 6 November 1997 the surface weather maps indicate that on 5 November 1997 at 0000 UTC (1900 LST), there was a low pressure center over eastern Kansas, high pressure building in from the northwest, and a cold front passing over the ARM SGP site. From 1200 UTC (0700 LST) 5 November to 1200 UTC (0700 LST) 7 November there were no strong synoptic-scale influences on the observational site. The surface weather map and the GOES IR image at 1200 UTC (0700 LST) on 6 November 1997 are presented in Fig. 4. The satellite image (Fig. 4a) shows that the clouds have a uniform appearance. The surface map (Fig. 4b) shows that there is no strong synoptic system over the observational site at this time and the surface pressure gradient over the SGP site is weak. Therefore, the conditions for these two cases may be considered suitable for studying nocturnal cloud formation over the SGP.

c. The observations and analysis of results

To organize our results, we first focus on the case of 6 November 1997. Figure 5 shows the cloud-base height observed by the ceilometer and the LCL calculated from surface meteorological data at the central facility on 5 and 6 November 1997. The observations show that the NBL clouds began forming at 2330 LST 5 November. A hint of the importance of local boundary layer influences on cloud formation can be seen from the clouds detected on the afternoon of 5 November. These clouds are the typical fair-weather cumulus clouds induced by convective thermals.

The mean vertical virtual potential temperature and specific humidity profiles at three different times (0030, 0630, and 0930 LST) on 6 November are shown in Fig.

TABLE 1. Observational instruments and systems at the ARM SGP site used in this study.

Instruments and systems	Acronyms	Properties
Belfort laser ceilometer	BLC	Cloud-base height
Micropulse lidar (low resolution)	MPL	Cloud-base height
Eddy Correlation Flux Measurement System	ECOR	Surface flux; U_*
Energy Balance Bowen Ratio System	EBBR	Surface flux; 3.4-m wind
Solar Infrared Radiation Observation Station	SIROS	Longwave radiative flux
Radio Acoustic Sounding System	RASS	Virtual temperature
Balloon-Borne Sounding System	BBSS	Wind, temperature, humidity
Surface Meteorological Observation System	SMOS	Wind (10 m), temperature (2 m), humidity (2 m), pressure (1 m)

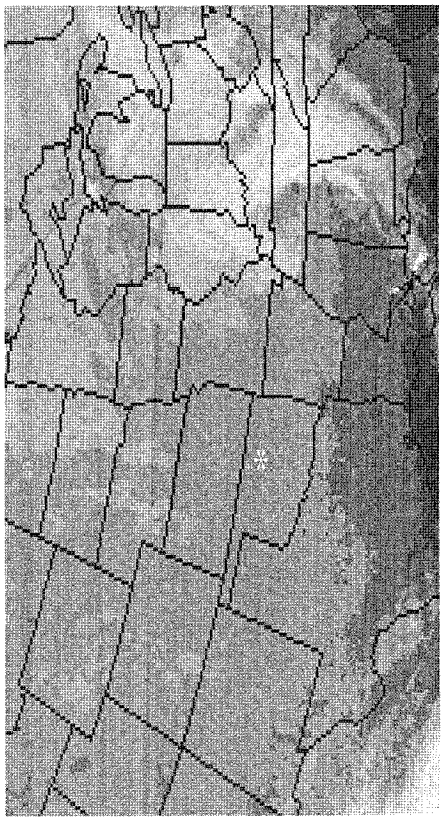

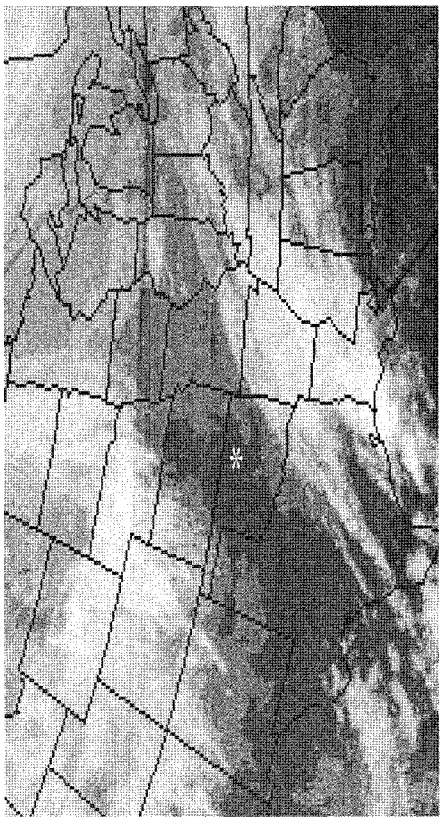

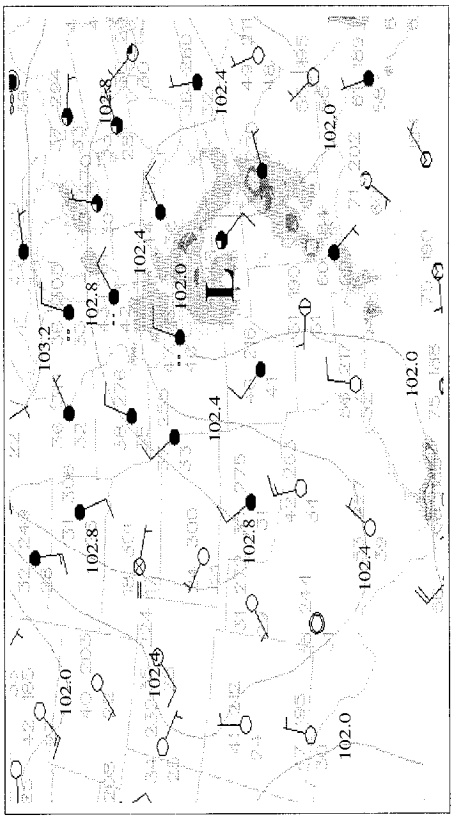

FIG. 4. As in Fig. 3, except at 1200 UTC (0700 LST) 6 Nov 1997.

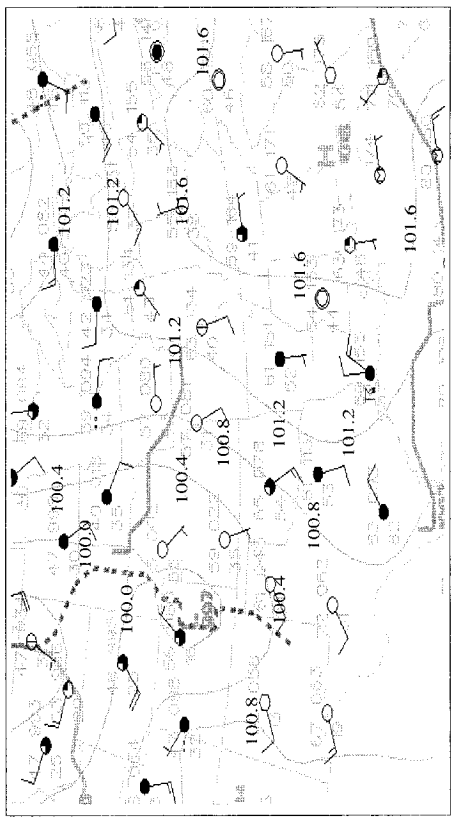

FIG. 3. GOES IR satellite image (upper panel) and the surface weather map (lower panel) at 0000 UTC (1900 LST) 25 Oct. 1996. The symbol * in the upper panel indicates the location of the SGP site. In the lower panel, plotted temperature and dewpoints are in degrees fahrenheit and pressure in tenths of kilopascals while contour intervals are 0.4 kPa.

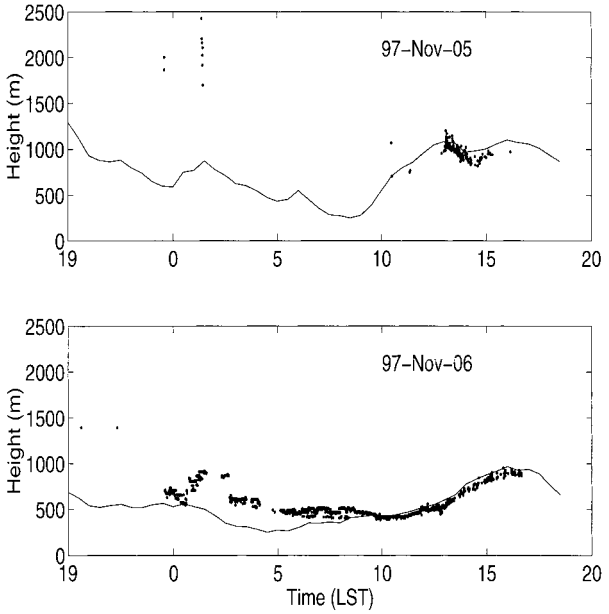

FIG. 5. The observed boundary layer cloud-base height on 5 Nov (upper panel) and 6 Nov (lower panel) 1997 at the ARM SGP central facility. Thin line: the LCL calculated from the surface meteorological data; dot: cloud-base height observed by the ceilometer.

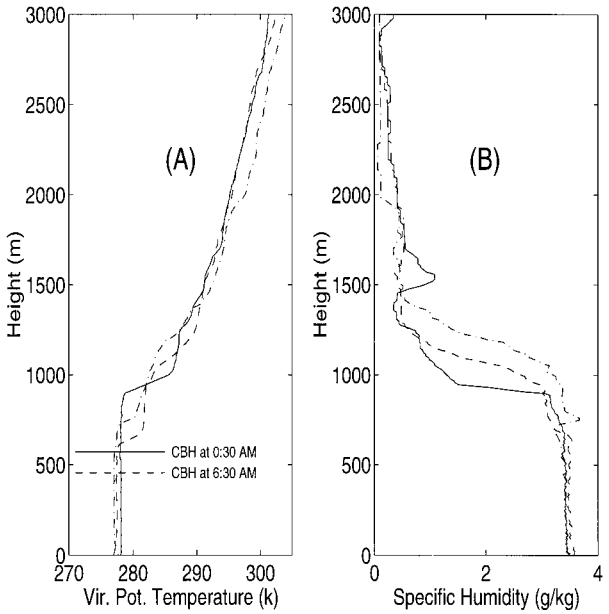

FIG. 6. Observed (a) virtual potential temperature and (b) specific humidity profiles on 6 Nov 1997 at the ARM SGP central facility. Solid line: 0030 LST; dashed line: 0630 LST; dash-dotted line: 0930 LST. The horizontal lines in (a) indicate the cloud-base height (CBH) detected by the ceilometer. The sounding data is from rawinsondes.

6. These profiles are obtained from the rawinsondes at the central facility. The virtual potential temperature profiles (Fig. 6a) show that beneath the top of the cloud there exists a well developed mixed layer that is not observed in the previous evening (5 November) or the day after (November 7). For these two nights, typical nocturnal stable boundary layer structures were observed and there were no clouds. An inversion with a virtual potential temperature increase of 5°–10°C tops the boundary layer at a height from 600 to 900 m on the evening of 6 November. The boundary layer thermodynamic structure in this evening was also detected by the Radio Acoustic Sounding System (RASS) at the central facility. The RASS observations (not shown here) show that the nocturnal mixed layer already existed before clouds formed. This kind of forced mixed layer structure may be related to the strong surface wind shear on this evening that we will show later.

The specific humidity profiles (Fig. 6b) also show a well-mixed layer beneath the cloud top that corresponds to the well-mixed virtual potential temperature profiles. Within the mixed layer the relative humidity (not shown here) increases almost linearly with height to the cloud base. The air above the mixed layer is very dry. There is a sharp jump across the inversion zone. This kind of structure also implies that the clouds forming in this evening are controlled by the local boundary layer processes.

The weak synoptic influence on this case is confirmed by Fig. 7, which shows the mean horizontal advective effects of temperature and humidity in the evening. We see that over the SGP site there is cold and dry advection in the surface layer, but this advection is very weak. The calculated advective tendency for both temperature and specific humidity at the central facility is less than 15% of the local change tendency during most of the evening on 6 November. Unfortunately, in this case we have only one sounding in the evening at the central facility, so that we have little information about advective effects in the lower troposphere. However, since the virtual potential temperature and specific humidity profiles from 1200 to 3000 m (shown in Fig. 6) have no substantial change from 0030 to 0630 LST, the horizontal advective effects should be very weak in the lower troposphere.

To examine the influence of surface heat fluxes on cloud formation, we compare the surface heat fluxes for the clear and cloudy evenings of this case, which is 5 and 6 November 1997. In this study, the surface sensible heat flux data were collected from both the Eddy Correlation Flux Measurement System (ECOR) and the Energy Balance Bowen Ratio System (EBBR), which were installed at different extended facilities of the SGP site. The ECOR data used in this study are collected at the CF1, E1, E6, E10, E16, and E24 facilities shown in Fig. 2 (the ECOR data from the other facilities are not available for this time period). A comparison between the ECOR and the EBBR using the data collected at the central facility shows that the fluxes observed by the two systems during the evening match reasonably well, although the fluctuations in the EBBR data are larger than those in the ECOR data (not shown here). Unfortunately, the surface latent heat flux data collected by

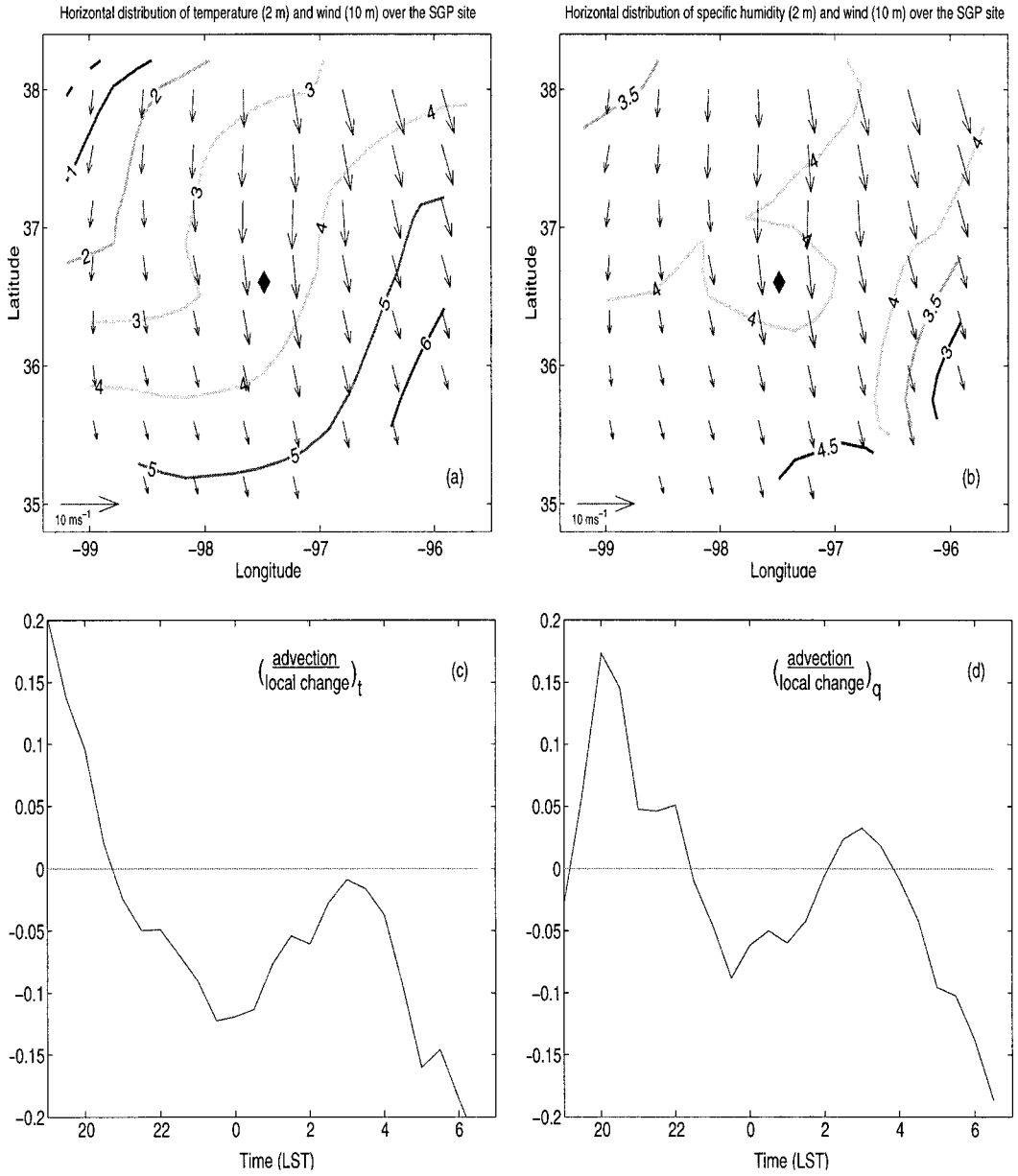

FIG. 7. The horizontal distribution of the (a) temperature (°C) and (b) specific humidity (g kg^{-1}) with surface wind fields from the Surface Meteorological Observation System (SMOS) at different facilities. The data are averaged from 1900 LST 5 Nov to 0700 LST 6 Nov. The diamond indicates the location of the central facility. The ratio between the advective tendency and the local change tendency for temperature (c) and specific humidity (d) at the central facility is calculated every half hour during this period.

the ECOR are not available for this period. Consequently, we can use only the latent heat flux data collected from the EBBR. Since the measurement of surface fluxes is much more difficult than that of mean variables such as temperature, pressure, and wind, the quality of flux data is usually not as good as other data. Random errors may occur from time to time. In this study we remove these erroneous data objectively by using a simple range filter. Since this analysis deals with flux data observed by many instruments at different facilities, systematic errors may also be introduced. To exclude systematic errors, we then intercompared the mean and standard deviation of these flux data (in time series) at different facilities to identify and eliminate unreliable flux data.

Figure 8 shows the averaged (1900–0700 LST) sensible and latent heat fluxes on 5 and 6 November, and the difference between them. Here the sensible heat fluxes are observed by the ECOR and the EBBR system, and the latent heat fluxes are from the EBBR system.

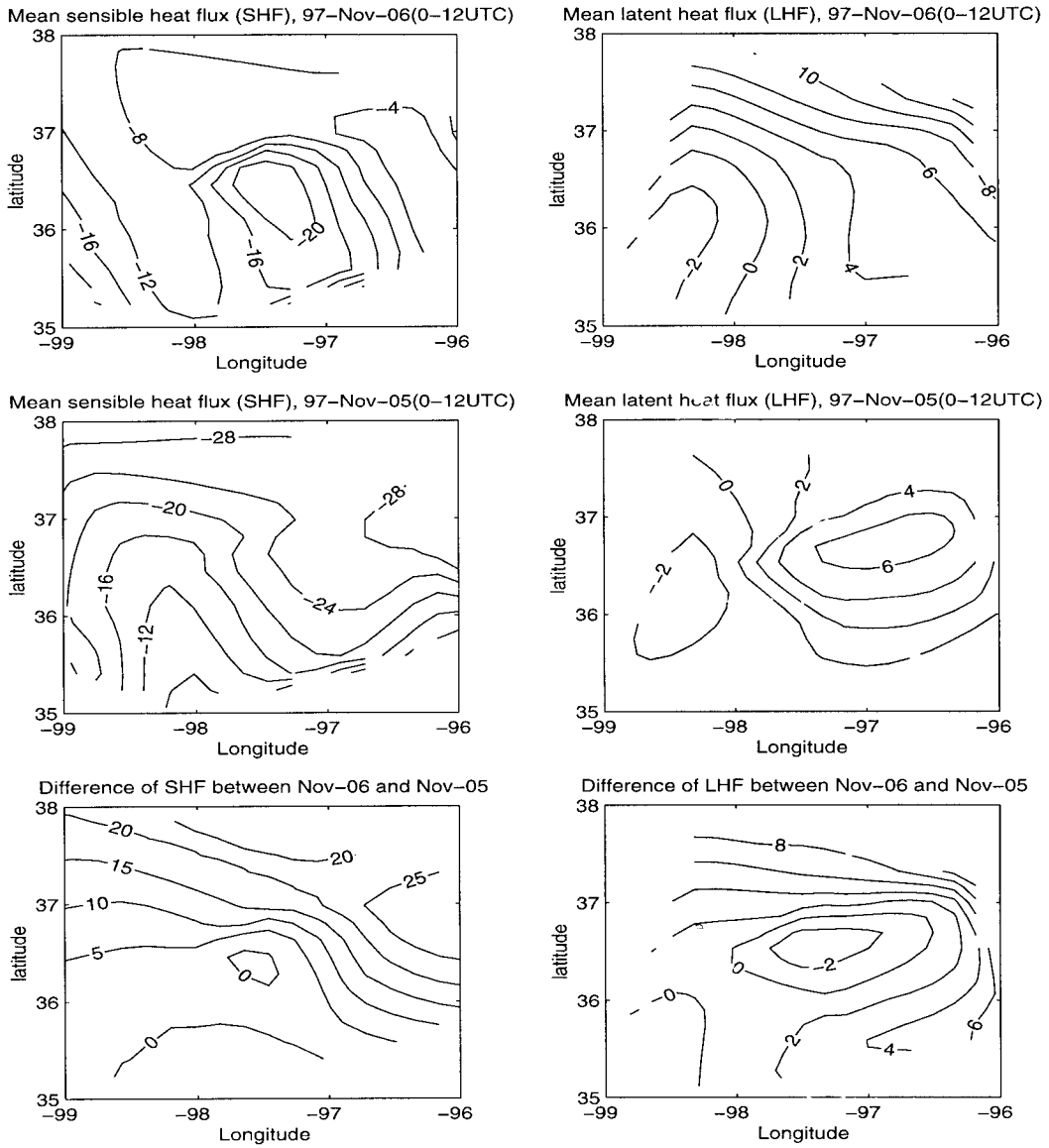

FIG. 8. Surface fluxes on 5 and 6 Nov 1997 averaged from 1900 to 0700 LST and their difference. (Units: W m^{-2}.) An upward flux is defined as positive. The sensible heat flux data is from the ECOR and the EBBR system, and the latent heat flux data is from the EBBR system.

To obtain the horizontal distribution of the surface heat flux, we used a triangle-based cubic interpolation method to interpolate the space irregular ECOR and EBBR data into the regular grids. Figure 8 indicates that on the cloudy evening (6 November) the downward sensible heat flux is relatively small, while the latent heat flux is relatively large compared with the clear evening (5 November) over the northeastern part of the research area. The observed distribution pattern and the magnitude of the surface fluxes indicate that compared with 5 November, 6 November has favorable conditions for the development of the nocturnal mixed layer and NBL cloud formation, since relatively strong surface evaporation helps the boundary layer stay moist while relatively weak downward sensible heat fluxes prevent the boundary layer from losing energy quickly to the surface. But from the figure, we also note that the surface fluxes in the central part of the research area are almost the same for these two evenings.

To more closely examine how the surface fluxes change with the development of the NBL in this area, we plot the time series of surface heat fluxes on the evening of 5 and 6 November at the central facility (Fig. 9). The observations show that there are only small differences between these two evenings, and these differences alone are not sufficient to explain why clouds formed more than 500 m aloft on 6 November over the central facility, while no clouds formed on the previous

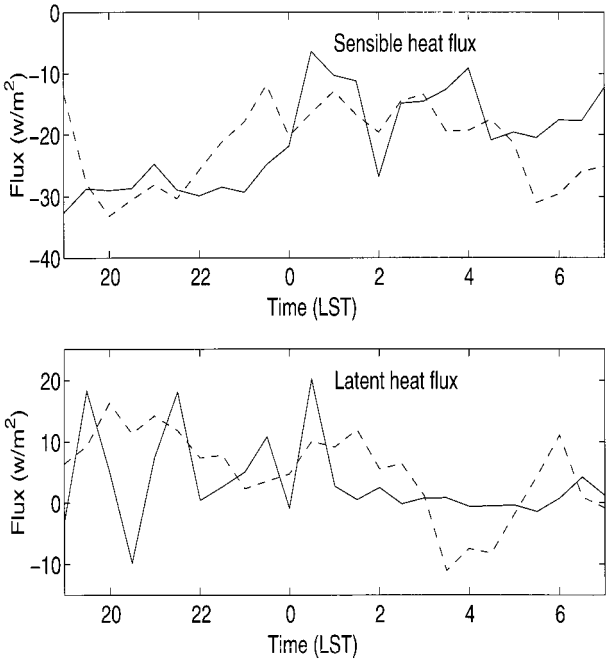

FIG. 9. Time series of observed sensible heat fluxes (measured by the ECOR) and latent heat fluxes (measured by the EBBR) on 5 Nov (dashed line) and 6 Nov (solid line), 1997 at the ARM SGP central facility. Here an upward flux is defined as positive.

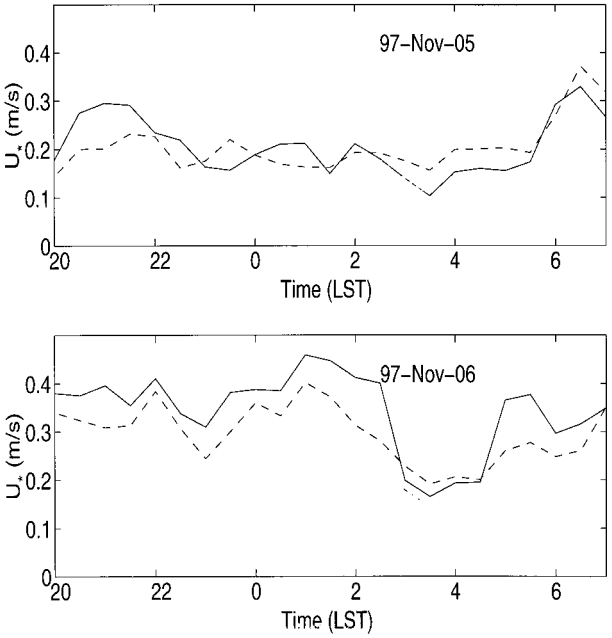

FIG. 10. Comparison of U_* between the eddy correlation method (solid line) and gradient method (dashed line) based on the data collected at the ARM SGP central facilities.

evening. Therefore, some other important processes must have been responsible for the cloud formation. The flux observations (Figs. 8 and 9) indicate that the surface flux may play an important role but does not play a unique role in the formation of NBL clouds. Thus the surface heat fluxes alone are not good indicators of the formation of NBL clouds.

The possible importance of surface wind shear for NBL cloud formation of this case can be seen by comparing the frictional velocity U_* for these two evenings. The frictional velocities that we used in this paper were provided by the ECOR system. For those facilities and those time periods when the ECOR data are not available, we calculated U_* using the Surface Meteorological Observation System (SMOS) 10-m wind data and the EBBR system 3.4-m wind data with the application of the Monin-Obukhov similarity theory—the so-called gradient method. We compared U_* from the gradient method with that from the direct method (ECOR) using the data collected at the central facility. Figure 10 shows one of these comparisons, and indicates that the gradient method provides a good estimate of the frictional velocity.

Figure 11 shows the averaged (1900–0700 LST) U_* on 5 and 6 November for the study area. To obtain this result, the same interpolation method was used as we used to produce Fig. 8. We see that U_* is much larger on 6 November than on 5 November especially in the northeastern part of the research area. Therefore, the surface wind shear may be a very important factor in triggering the formation of clouds.

The observed surface and boundary layer features indicate that both thermodynamic and dynamic pro-

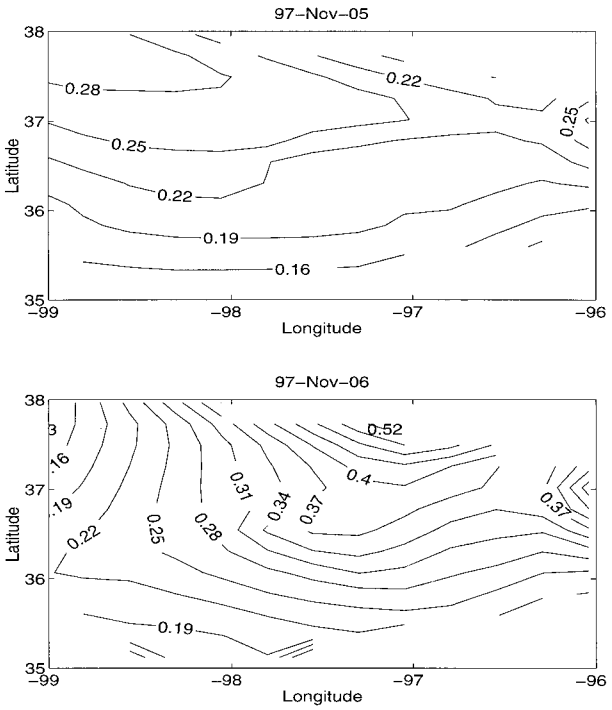

FIG. 11. Horizontal distribution of the frictional velocity U_* averaged from 1900 to 0700 LST on 5 and 6 Nov 1997.

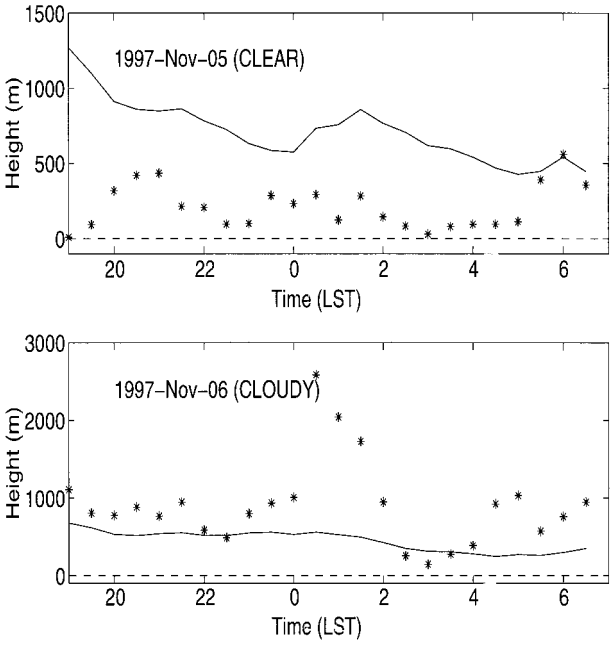

FIG. 12. The calculated LCL (line) and the critical level $h_{critical}$ (star) on 5 and 6 Nov 1997 at the ARM SGP central facility.

cesses in the boundary layer may influence the formation of NBL clouds. According to our analysis, the relative importance of these different processes can be evaluated by the ratio between the LCL and the critical level. To evaluate the result [Eq. (18)] we obtained in section 2, we calculated the LCL and the critical level on 5 and 6 November (Fig. 12). We see that for the evening of 5 November, a time when there is no cloud, the LCLs are higher than the critical levels, while on 6 November, when the NBL clouds did form and develop, the LCLs are lower than the critical levels. These results are consistent with the arguments made in section 2.

Since surface inhomogeneities may impact cloud formation, we calculated the LCLs and the critical levels at all the available observational facilities in the research area on 5 and 6 November (Fig. 13). Here the calculation was averaged over the whole night (1900–0700 LST). On 5 November, there is no cloud recorded, and as we expected the critical levels, which are indicated by star-bars, are lower than the LCLs, which are represented by the scaled surface in Fig. 13, over the whole research area. On 6 November, however, when clouds were recorded near the central facility, we see that for most of the areas, the critical levels are higher than the LCLs. These results can be mostly attributed to the strong wind shear on 6 November that we showed in Fig. 11, but also can be partly attributed to the weak surface sensible heat flux on the evening of 6 November (shown in Fig. 8). However, along the southwest boundary of the research area, the critical levels are lower than the LCLs. This indicates less probability for clouds in this region. Unfortunately, we do not have direct cloud observation at these facilities. Instead, we examine the downward longwave radiative flux data to determine if low clouds exist or not. Figure 14 shows the time series of downward longwave radiative flux measured by the Solar Infrared Radiation Observation Stations (SIROS) at the different facilities. For those facilities (see Fig. 2 for locations) where the critical levels are lower than the LCLs, the downward longwave radiative flux is small, below 250 W m^{-2}, which is a typical value for the clear sky during this season. However, for those facilities where the critical levels are higher than the LCLs, the downward longwave radiative flux is large, around 340 W m^{-2}, which is consistent with the presence of low clouds. These observations indicate that the relationship between the LCL and the critical level is a sensitive indicator of whether the clouds exist or not and may adequately represent the basic physics for nocturnal cloud formation. Here, the influence of wind shear for triggering cloud formation can be easily seen by comparing Figs. 11, 12 and 13. On 6 November, U_* is much smaller in areas where there is no cloud than in areas where clouds formed.

The influence of boundary layer processes on the formation of NBL clouds can be illustrated by another set of observations obtained on 25 October 1996. Figure 15 shows the cloud-base height from the ceilometer at the central facility, the LCL, and the critical level calculated from the SMOS and the ECOR systems on the evening of 25 October. We see that the clouds formed in the middle of the night on 25 October, and the relation between calculated LCLs and the critical levels once again matches our analysis well. For the cloudy night the critical level is higher than the LCL.

Figure 16 shows that the virtual potential temperature and specific humidity profiles on 25 October at the central facility. Compared with the first case (Fig. 6), we see that a much stronger and sharper inversion caps the well-mixed boundary layer on 25 October. The humidity profiles show that the boundary layer is more moist than the 6 November 1997 case, and that the air above the inversion is very dry.

To further examine whether the ratio between the LCL and the critical level is a key parameter for the formation of nocturnal stratus clouds, we studied all the clear cases with little or no synoptic influence (obtained by subjective examination of surface weather maps, satellite images, and surface pressure tendency) observed in 1997. We calculated the LCL and the critical level every 30 min during the evening from 1900 to 0700 LST for all 55 cases (Fig. 17). As we expected, almost all the calculated LCLs are larger than the critical levels in all of these cases. This calculation confirms that regardless of the strength of NBL stability, as long as the critical level is lower than the LCL, it is difficult to form NBL clouds.

To illustrate the general variation of the LCL and the critical level under clear evening conditions, we select two cases with three consecutive clear-sky evenings and

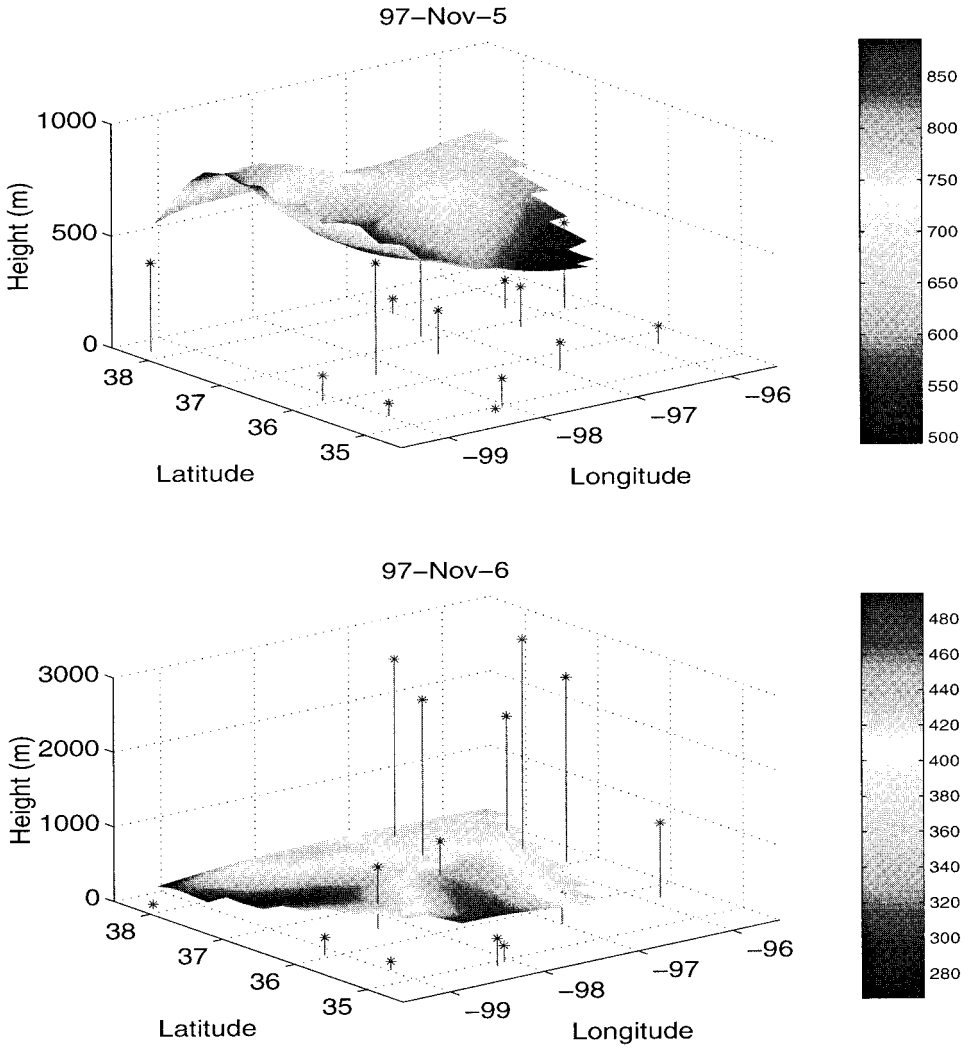

FIG. 13. The averaged LCL from 1900 to 0700 LST (scaled surface) and the critical level (bar-star) over the whole ARM SGP research area.

then plot the time series of the LCL and the critical level (Fig. 18). Although there is no fixed pattern for the evolution of the critical level, the LCL variation does show an interesting pattern that consists of a rapid decrease right after sunset and a rather steady-state period till the next morning before sunrise. The reason for this is that temperature falls more rapidly than moisture. In fact, the surface moisture may increase slightly due to the increase of stable stratification near the surface while evaporation continues. Here we can see that due to the strong stability of the NBL (the small value of h_{critical} that is proportional to the Monin-Obukhov length scale), the turbulence in the NBL is suppressed. The weak turbulence can not mix the low-level atmosphere up to a depth that exceeds the LCL, and clouds cannot form at the boundary layer top. Therefore, the wind shear, especially surface wind shear (also, a major mechanism for the maintenance of the mixed layer above the surface layer), is extremely important for the formation of NBL clouds. Stronger wind shear will result in a thicker NBL, which can be evaluated by the critical level as we showed in section 2.

5. Conclusions and discussions

Although continental NBL clouds can form for a variety of reasons, it is apparent that the land surface and boundary layer processes play a fundamental role in the formation and evolution of these clouds. Based on simple well-mixed boundary layer theory, we assume that the basic condition for the formation of NBL clouds is that the LCL is lower than the boundary layer depth. An analysis of the deepening rate of the mixed layer based on the TKE budget averaged over the NBL indicates that an important parameter for the formation of NBL clouds is the ratio of the LCL and the critical level, which is proportional to the Monin-Obukhov length scale. This ratio fundamentally controls the formation

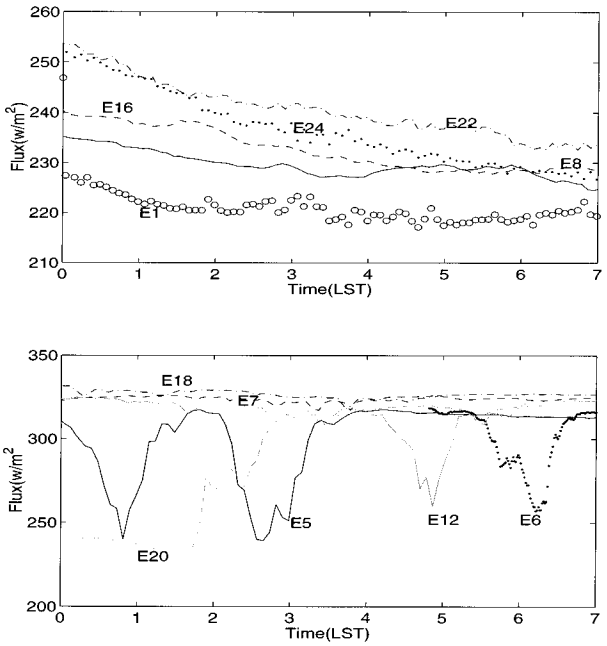

FIG. 14. Observed downward longwave radiative fluxes by the Solar Infrared Radiation Observation Station (SIROS) at different facilities. The locations of the facilities are shown in Fig. 2.

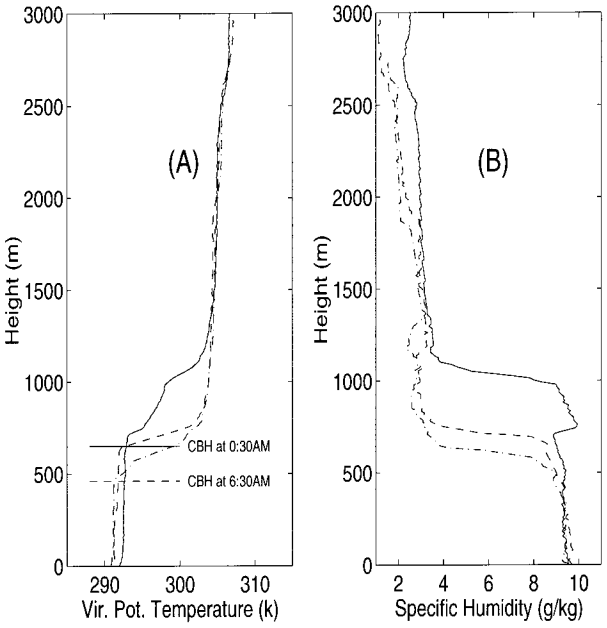

FIG. 16. Observed (a) virtual potential temperature and (b) specific humidity profiles on 25 Oct 1996 from the SGP ARM central facility. Solid line: 0030 LST; dashed line: 0630 LST; dash-dotted line: 0930 LST. The horizontal lines in (a) indicate the cloud-base height (CBH) detected by the ceilometer. The sounding data are from rawinsondes.

of NBL clouds. If the LCL is higher than the critical level, then it is impossible to form clouds. However, if the LCL is below the critical level, then the formation of clouds is possible.

The data collected from the ARM SGP site are used in this study to examine the results of our theoretical analysis. The case studies show that wind shear can be an important factor in the formation of NBL clouds. To confirm the analysis made in this study, we also simulated the case of 6 November 1997 using the RAMS

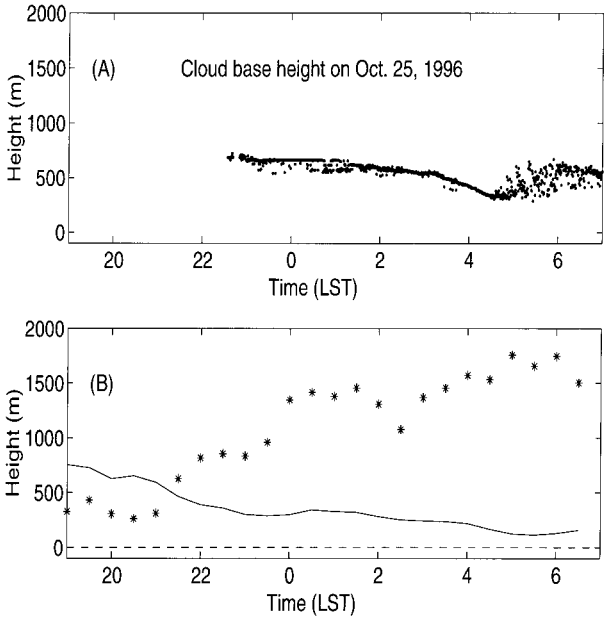

FIG. 15. (a) The observed boundary layer cloud-base height by the ceilometer on 25 Oct 1996. (b) The calculated LCL (thin line) and the critical level (star) at the ARM SGP central facility.

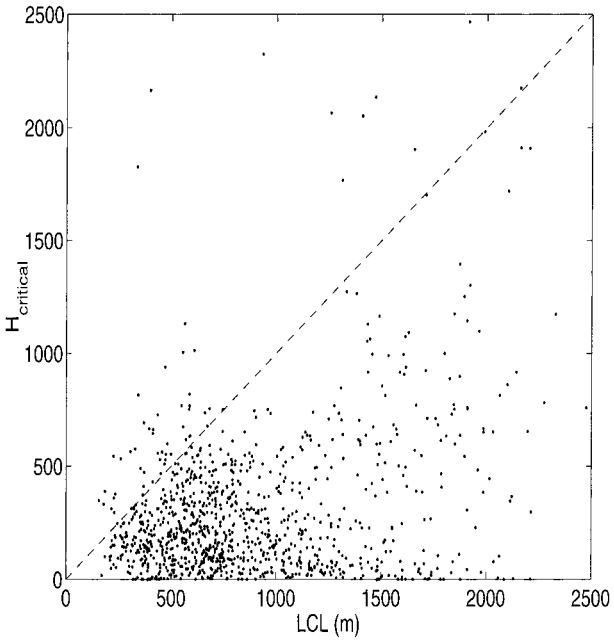

FIG. 17. The calculated LCL vs the critical level (every half hour from 1900 to 0700 LST) for all the 55 clear evening cases with little synoptic influence in 1997.

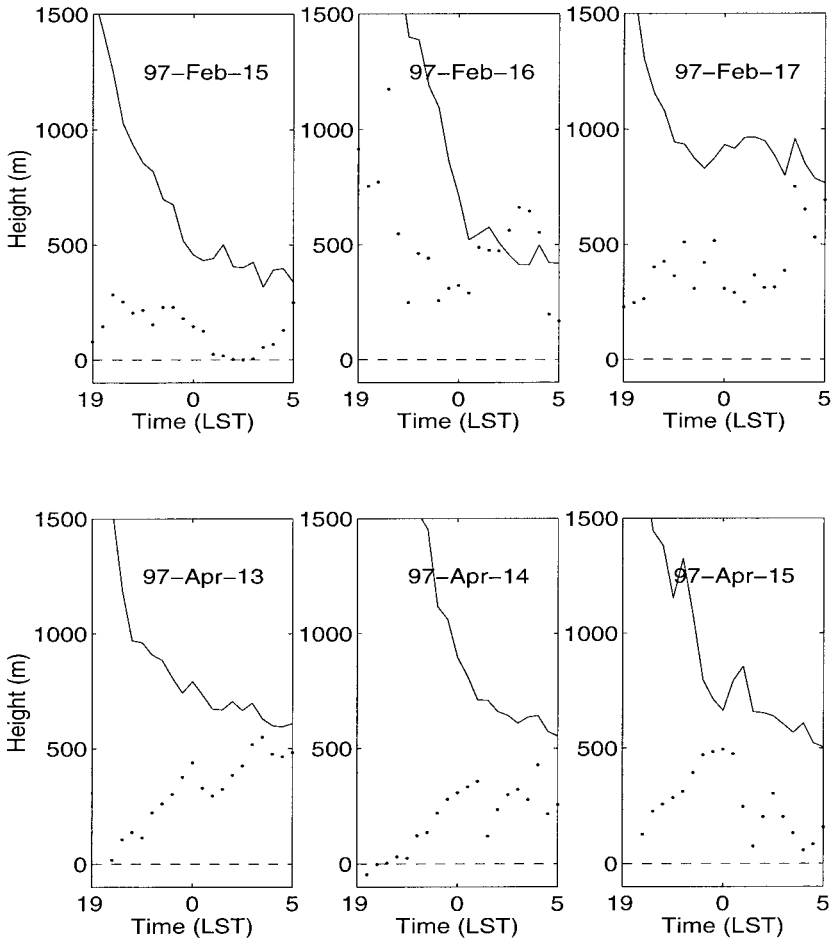

FIG. 18. The time series of the LCL (line) and the critical level (dot) for the two cases of three consecutive clear evenings (15, 16, 17 Feb and 13, 14, 15 Apr 1997).

model. The model was initialized using rawinsondes and surface observations collected at 1230 LST 5 November from the central and the four boundary facilities. A comparison between simulations and observations shows that the model reproduces the real atmosphere reasonably well (not shown here). The analysis of the heat and moisture budget using model output shows that the effect of advection is very weak compared with the turbulent transports. The moisture transport due to the turbulence was significant before cloud formation, which indicates that the advection is a secondary effect for the formation of NBL clouds in this case.

The formation of NBL clouds and the cloud-topped boundary layer is a relatively poorly understood issue compared with a clear stable boundary layer where a local similarity theory has been developed (e.g., Nieuwstadt 1984; Sorbjan 1986; Rogers et al. 1995a). According to this study, a shear-driven boundary layer provides a favorable environment for the formation of NBL clouds. However, since the interaction of gravity waves and the turbulent eddies induced by shear production adds a further complication to this problem, the real situation should be much more complicated than we treat here. However, a simple theory is needed to elucidate the basic physics.

Another important process related to this problem is the longwave radiative cooling at cloud top, a factor that can be critical after clouds form. The scenario supported in this study is that strong wind shear produces sufficient turbulent mixing to provide an upward transport of moisture, a key factor for triggering cloud formation. As soon as clouds form, the longwave radiative cooling at the cloud top can generate turbulence, a process called convective instability induced by radiative cooling. At this stage, the growth rate of the mixed layer is controlled not only by shear and the stable stratification, but also by longwave radiative cooling at the cloud top. The vertical longwave radiative flux data shown by Duynkerke et al. (1995) indicate the importance of longwave radiative cooling at the cloud top for the cloud development. However, since radiative processes depend on many factors, such as the distribution of water vapor and liquid water in the clouds, the fractional cloud cover, the gradient of liquid water, and water

vapor above the boundary layer, substantial work is needed to understand the role of radiative processes in the development of boundary layer clouds and to parameterize it appropriately in numerical models.

Acknowledgments. This research was supported by the Department of Energy under Grant DEFG0297ER62337. The data used in this paper were obtained from the ARM Data Archive. We thank Dr. Fujio Kimura for providing us with the RAMS model, and Dr. Hongli Jiang for discussing Deardorff's turbulent closure scheme. We are also grateful to the anonymous reviewers for their careful reading of the manuscript and their many constructive comments.

REFERENCES

Albrecht, B. A., 1979: A model of the thermodynamic structure of the trade-wind boundary layer. Part II: Applications. *J. Atmos. Sci.,* **36,** 90–98.

——, D. A. Randall, and S. Nicholls, 1988: Observation of marine stratocumulus clouds during FIRE. *Bull. Amer. Meteor. Soc.,* **69,** 618–636.

——, C. S. Bretherton, and D. Johnson, 1995: The Atlantic stratocumulus transition experiment—ASTEX. *Bull. Amer. Meteor. Soc.,* **76,** 889–904.

Andre, J. C., G. De Moor, P. Lacarrere, G. Therry, and R. Du Vachat, 1978: Modeling the 24-hour evolution of the mean and turbulent structures of the planetary boundary. *J. Atmos. Sci.,* **35,** 1861–1883.

Betts, A. K., 1973: Nonprecipitating cumulus convection and its parameterization. *Quart. J. Roy. Meteor. Soc.,* **99,** 178–196.

Businger, J. A., J. C. Wyngaard, Y. Izumi, and E. F. Bradley, 1971: Flux profile relationships in the atmospheric surface layer. *J. Atmos. Sci.,* **28,** 181–189.

Caughey, S. J., J. C. Wyngaard, and J. C. Kaimal, 1979: Turbulence in the evolving stable boundary layer. *J. Atmos. Sci.,* **36,** 1041–1052.

Chou, S.-H., D. Atlas, and E.-N. Teh, 1986: Turbulence in a convective marine atmospheric boundary layer. *J. Atmos. Sci.,* **43,** 547–564.

Deardorff, J. W., 1974: Three-dimensional numerical study of turbulence in an entraining mixed layer. *Bound.-Layer Meteor.,* **7,** 199–226.

——, 1980: Stratocumulus-capped mixed layers derived from a three-dimensional model. *Bound.-Layer Meteor.,* **18,** 495–527.

——, G. E. Willis, and B. H. Stockton, 1980: Laboratory studies of the entrainment zone of a convectively mixed layer. *J. Fluid Mech.,* **100,** 41–64.

Del Genio, A. D., N.-S. Yao, W. Kovari, and K.K. -W. Lo, 1996: A prognostic cloud water parameterization for general circulation models. *J. Climate,* **9,** 270–304.

Duynkerke, P. G., H. Q. Zhang, and P. J. Jonker, 1995: Microphysical and turbulent structure of nocturnal stratocumulus as observed during ASTEX. *J. Atmos. Sci.,* **52,** 2763–2777.

Garratt, J. R., 1987: The stably stratified internal boundary layer for steady flow and diurnally varying offshore flow. *Bound.-Layer Meteor.,* **38,** 369–394.

——, 1992: *The Atmospheric Boundary Layer*. Cambridge University Press, 316 pp.

Kraus, E. B., 1977: *Modeling and Prediction of the Upper Layers of the Ocean.* Pergamon Press, 143 pp.

——, and J. S. Turner, 1967: A one-dimensional model of the seasonal thermocline. II. The general theory and its consequences. *Tellus,* **19,** 98–106.

Lenschow, D. H., 1974: Model of the height variation of the turbulence kinetic energy budget in the unstable planetary boundary layer. *J. Atmos. Sci.,* **31,** 465–474.

Lilly, D. K., 1968: Models of cloud-topped mixed layers under a strong inversion. *Quart. J. Roy. Meteor. Soc.,* **94,** 292–309.

Louis, J. F., 1979: A parametric model of vertical eddy fluxes in the atmosphere. *Bound.-Layer Meteor.,* **17,** 187–202.

Mellor, G. L., and T. Yamada, 1982: Development of a turbulence closure model for geophysical fluid problems. *Rev. Geophys. Space Phys.,* **20,** 851–875.

Moeng, C.-H., 1984: A large-eddy simulation for the study of planetary boundary layer turbulence. *J. Atmos. Sci.,* **41,** 2052–2062.

——, 1986: Large-eddy simulation of a stratus-topped boundary layer. Part I: Structure and budgets. *J. Atmos. Sci.,* **43,** 2886–2900.

——, S. Shen, and D. A. Randall, 1992: Physical processes within the nocturnal stratus-topped boundary layer. *J. Atmos. Sci.,* **49,** 2384–2401.

——, P. P. Sullivan, and B. Stevens, 1999: Including radiative effects in an entrainment rate formula for buoyancy-driven PBLs. *J. Atmos. Sci.,* **56,** 1031–1049.

Nieuwstadt, F. T. M., 1984: The turbulence structure of the stable nocturnal boundary layer. *J. Atmos. Sci.,* **41,** 2202–2216.

Pielke, R. A., and Coauthors, 1992: A comprehensive meteorological modeling system—RAMS. *Meteor. Atmos. Phys.,* **49,** 69–91.

Rogers, D. P., D. W. Johnson, and C. A. Friehe, 1995a: The stable internal boundary layer over a coastal sea. Part I: Airborne measurement of the mean and turbulence structure. *J. Atmos. Sci.,* **52,** 667–683.

——, X. Yang, and P. M. Norris, 1995b: Diurnal evolution of the cloud-topped marine boundary layer. Part I: Nocturnal stratocumulus development. *J. Atmos. Sci.,* **52,** 2953–2966.

Sorbjan, Z., 1986: On similarity in the atmospheric boundary layer. *Bound.-Layer Meteor.,* **34,** 377–397.

——, 1987: An examination of local similarity theory in the stably stratified boundary layer. *Bound.-Layer Meteor.,* **38,** 63–71.

——, 1999: Similarity of scalar fields in the convective boundary layer. *J. Atmos. Sci.,* **56,** 2212–2221.

Stephen, A. K., and D. L. Hartmann, 1993: The seasonal cycle of low stratiform clouds. *J. Climate,* **6,** 1587–1606.

Stevens, B., W. R. Cotton, G. Feingold, and C.-H. Moeng, 1998: Large-eddy simulations of strongly precipitating, shallow, stratocumulus-topped boundary layers. *J. Atmos. Sci.,* **55,** 3616–3638.

Stull, R. B., 1985: A fair-weather cumulus cloud classification scheme for mixed-layer studies. *J. Climate Appl. Meteor.,* **24,** 49–56.

——, 1988: *An Introduction to Boundary Layer Meteorology.* Kluwer Academic Publishers, 665 pp.

Therry, G., and P. Lacarrere, 1983: Improving the eddy kinetic energy model for planetary boundary layer description. *Bound.-Layer Meteor.,* **25,** 63–88.

Wang, S.-P., 1993: Modeling marine boundary-layer clouds with a two-layer model: A one-dimensional simulation. *J. Atmos. Sci.,* **50,** 4001–4021.

Wyngaard, J., 1975: Modeling the planetary boundary layer extension to stable case. *Bound.-Layer Meteor.,* **9,** 441–460.

Zeman, O., 1979: Parameterization of the dynamics of the stable boundary layer and nocturnal jets. *J. Atmos. Sci.,* **36,** 792–804.

Zhou, M. Y., D. H. Lenschow, B. B. Stankov, J. C. Kaimal, and J. E. Gaynor, 1985: Wave and turbulence structure in a shallow baroclinic convective boundary layer and overlying inversion. *J. Atmos. Sci.,* **42,** 47–57.